Experimental Study of the Mechanical Properties of a Spherical Parallel Link Mechanism With Arc Prismatic Pairs

Naoto Saiki, Kenjiro Tadakuma, Masahiro Watanabe, Kazuki Abe, Masashi Konyo, and Satoshi Tadokoro

***Abstract*—A two-degrees-of-freedom spherical parallel link mechanism (2-DOF SPM) was designed to ensure that it only has rotational degrees of freedom in two directions around a fixed center. In general, 2-DOF SPM includes passive rotating pairs, and at least two actuators are needed to change the end-effector posture. The arrangement of the links and pairs determines the characteristics and performance of SPM, so 2-DOF SPMs were designed considering various requirements, such as output torque, accuracy, and space constraints for applications. To satisfy these requirements, arc prismatic pairs can be used in SPMs. In order to use in SPMs, as for arc prismatic pairs, the concrete configuration and design methods for arc prismatic pairs have been studied. Furthermore, in order to compensate for the influence of friction on the positioning error, the control model considering the friction has been proposed by constructing a feedback loop containing experimentally found parameters. However, the conventional model is not a mechanical model of friction. Therefore, it is not suitable for calculating the friction force and understanding how the limit of the workspace changes due to the influence of friction. In this study, we construct a mechanical friction model considering the intersection angle change between the input and the rail slide direction. In addition, using the friction model, we clarify the influences of friction on the workspace and driving the SPM to realize high-performance 2-DOF SPM. First, we theoretically clarified the influence of friction on the workspace by considering the case of a slider-type differential-drive 2-DOF SPM. Second, the driving torque was experimentally measured, and the influence of friction on driving was examined.**

***Index Terms*—Mechanism design, actuation and joint mechanisms, parallel robots.**

Manuscript received 24 February 2022; accepted 28 June 2022. Date of publication 20 July 2022; date of current version 29 August 2022. This letter was recommended for publication by Associate Editor C.-H. Kuo and Editor C. Gosselin upon evaluation of the Reviewers' comments. *(Naoto Saiki, Kenjiro Tadakuma and Masahiro Watanabe contributed equally to this work.) (Corresponding author: Kenjiro Tadakuma.)*

Naoto Saiki, Masashi Konyo, and Satoshi Tadokoro are with the Graduation School of Information Sciences, Tohoku University, Sendai, Japan (e-mail: siknot.zgmf.x20a.sfg@gmail.com; konyo@rm.is.tohoku.ac.jp; tadokoro@rm.is.tohoku.ac.jp).

Kenjiro Tadakuma is with the Graduation School of Information Sciences and Tough Cyberphysical AI Research center, Tohoku University, Sendai, Japan (e-mail: tadakuma@rm.is.tohoku.ac.jp).

Masahiro Watanabe and Kazuki Abe are with the Tough Cyberphysical AI Research center, Tohoku University, Sendai, Japan (e-mail: watanabe.masahiro@rm.is.tohoku.ac.jp; kazuki.abe.org@gmail.com).

Digital Object Identifier 10.1109/LRA.2022.3192760

I. Introduction

THE two-degrees-of-freedom spherical parallel link mechanism (2-DOF SPM) is designed to limit the degree of freedom of the end-effector to only two-directional motion around a fixed center [1]. It is suitable for applications that need to change the end-effector posture while always aimed at the control target at the fixed center [2], [3], such as tracking [4], [5], wrist or ankle joints of humanoid robots [6]–[9], surgical robots [10], and stabilization platforms [11]–[13].

2-DOF SPM has the advantages below compared with 2-DOF spherical serial link mechanism because 2-DOF SPM is one of the parallel link mechanisms; 1) the drive torque can be distributed to multiple actuators and the torque required for each actuator can be reduced, 2) the mechanism can be highly accurate because errors due to link deformation are averaged without accumulation owing to the closed-loop link structure, 3) it is easy to modularize the components and make the structure symmetric, thus simplifying the placement of the center of gravity at the center of the mechanism [14], [15].

One of the important aspects of the 2-DOF SPM is the range of motion. In general, 2-DOF spherical serial mechanism [16] tend to have a wide workspace, but 2-DOF SPM have the disadvantage of a small workspace and singular postures with an indefinite mechanical shape. In 2-DOF SPM, the workspace is closely related to but singularity also component collision. The components in the parallel link mechanism cause more collision owing to the closed-loop link structure [17].

Therefore, analytical and mechanical approaches have been studied to expand the workspace [18]–[21]. As an example of a mechanical approach, a curved biaxial swing mechanism has been proposed, in which two input rotary shafts are arranged coaxially and a differential drive is used to eliminate component collision in one direction [22]. Consequently, a 360° infinite rotation was realized without component interference in the roll direction.

In addition to the workspace, 2-DOF SPMs are designed by considering various requirements for applications, such as output torque, accuracy, and space constraints. To satisfy these requirements and clear the constraints, arc prismatic pairs (arc sliders) can used [10], [22]. Furthermore, arc prismatic pairs are also used in 3-DOF SPM [23]. These have studied the concrete

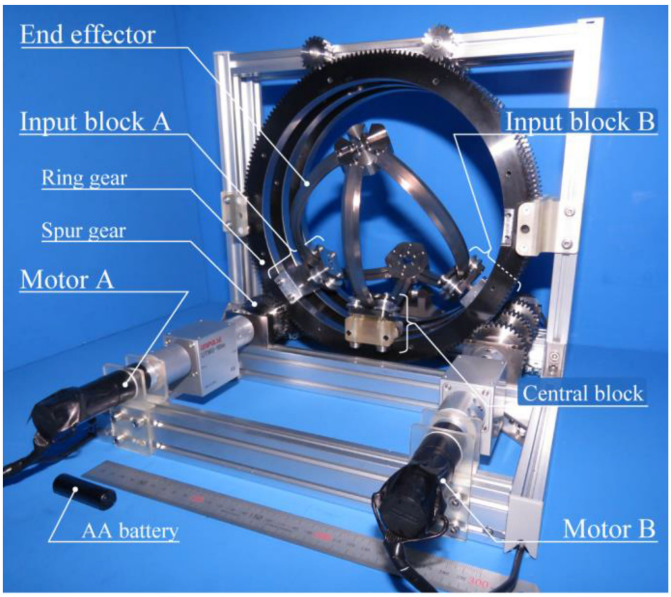

Fig. 1. Physical prototype embodying a 2-DOF SPM with arc prismatic pairs driven by a differential drive.

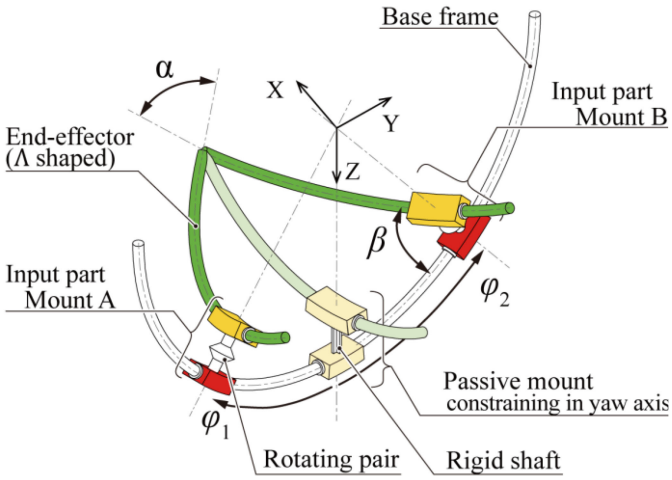

Fig. 2. Link and pair arrangement in the proposed "curved biaxial swing biaxial mechanism". In the input blocks A and B, lower arc prismatic pairs are active rotating pairs. The other upper arc prismatic pairs and middle rotating pairs are passive rotating pairs.

configuration and design methods for arc prismatic pairs used in SPMs.

In these arc prismatic pairs, Kang et al. constructed a feedback loop containing experimentally found parameters and proposed the control model considering the friction in order to compensate for the influence of friction on the positioning error [24].

However, the model is not a mechanical model of friction. Therefore, it is not suitable for calculating the friction force and understanding how the limit of the workspace changes due to the influence of friction.

In this study, we construct a mechanical friction model considering the intersection angle change between the input and the rail slide direction. In addition, using the friction model, we clarify the influences of friction on the workspace and driving the SPM to realize high-performance 2-DOF SPM.

In Section II, we first introduced the slider-type differential -drive 2-DOF SPM to confirm the workspace of the SPM without considering the influence of friction. In Section III, friction resistance of the arc prismatic pair is considered and the influence of friction on the workspace is clarified. In Section IV, the torque transmission ratio of the SPM is calculated to understand the input-output characteristics during pitch motion of the SPM. In Section V, we considered the specific configuration design of the arc prismatic pair and fabricated a metal prototype of a 2-DOF SPM with arc prismatic pairs driven by a differential drive, as shown in Fig. 1. In Section VI, the actual driving torque was measured experimentally using a metal prototype. Finally, Section VII concludes the study and presents the scope for future research.

II. Slider-Type Differential Drive 2-DOF SPM

The curved biaxial swing mechanism developed by the authors is a slider-type 2-DOF SPM that enables the output pitch motion by a differential drive around the Y-axis, as shown in Fig. 2. The SPM refers to the slider-type 2-DOF planar parallel link mechanism [25] based on prismatic pairs and a differential drive.

The SPM is devised by replacing the translational output motions in the planar mechanism with rotational output motions. Although the type of output motion is changed, the risk of component interference remains low because the input axes of the differential mechanism are arranged in parallel and coaxially without crossing each other. Consequently, no interference occurs in the input blocks during rolling.

A. Link and Joint Arrangement

The proposed mechanism consists of eight rotational pairs, including arc prismatic pairs, and three kinematic chains (RR-RRR-RRR). The end-effector comprises three arc rails that are crossed and connected at equal intervals.

As the result, the RR chain is always located in the center of the two RRR chains, that is, the proposed mechanism is symmetry. In addition, All the mounts and the end effector rotate on spherical surfaces centered on the origin O.

B. Motion

When the input blocks A and B are rotated in the same direction and speed, a roll rotation output around the X-axis is obtained. However, when input blocks A and B are rotated in the opposite direction at the same speed, the respective rails of the end-effector slide out and the pitch rotation output around the Y-axis is obtained.

C. Workspace

The workspace of the mechanism has already been clarified based on the geometrical relationships of the mounts' position and the end effector [22], as shown in (1) by considering the geometrical conditions of the shape and position of each part,

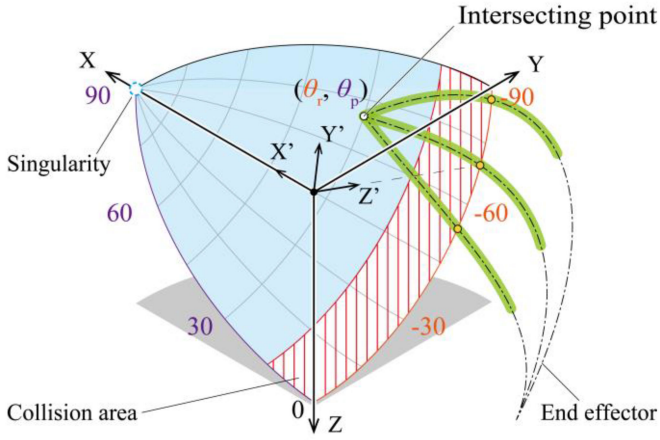

Fig. 3. Range of motion of the end-effector in the XYZ coordinate system. The light blue area is the workspace that the rail intersection point of the end-effector can reach.

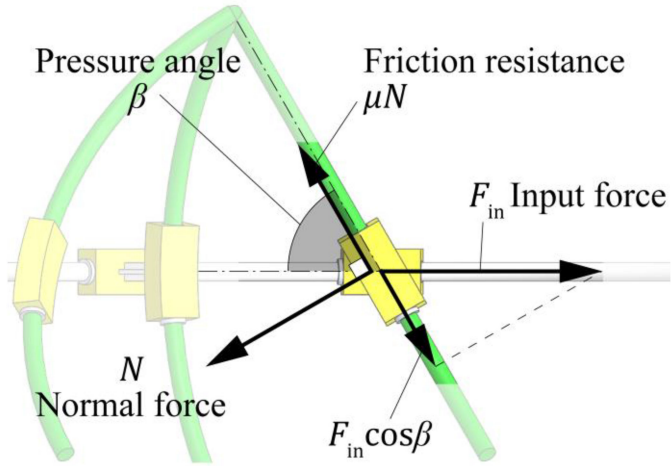

Fig. 4. Rail sliding condition for the arc prismatic pair in the input block B (μ: Friction coefficient, β: Pressure angle). .

as shown in Fig. 3. In (1), θ_{r} and θ_{p} represent the roll and pitch rotation angle of the end effector.

$$\begin{cases} \theta_r = \frac{\varphi_1+\varphi_2}{2}. \\ \theta_p = \sin^{-1}\left(\frac{\tan\frac{\varphi_1-\varphi_2}{2}}{\tan\frac{\alpha}{2}}\right). \end{cases} \tag{1}$$

Further, the end effector's posture can be described using the X–Y–Z Euler angles, similar to when describing the attitude of the two-joint serial link robot [26]. This is because the end effector in this mechanism rotates -θ_{r} around the X-axis and then θ_{p} around the Y'-axis on the rotated X'Y'Z' axis, as shown in Fig. 3. The posture in this condition can be described as in (2), using θ_{r} and θ_{p}.

$$\begin{aligned} {}^{A}_{B}R_{X'Y'Z'} &= R_X\left(-\theta_{\mathrm{r}}\right) R_Y\left(\theta_{\mathrm{p}}\right) R_Z\left(0\right) \\ &= \begin{bmatrix} \cos\theta_{\mathrm{p}} & 0 & \sin\theta_{\mathrm{p}} \\ -\sin\theta_{\mathrm{r}}\sin\theta_{\mathrm{p}} & \cos\theta_{\mathrm{r}} & \sin\theta_{\mathrm{r}}\cos\theta_{\mathrm{p}} \\ -\cos\theta_{\mathrm{r}}\sin\theta_{\mathrm{p}} & -\sin\theta_{\mathrm{r}} & \cos\theta_{\mathrm{r}}\cos\theta_{\mathrm{p}} \end{bmatrix}. \end{aligned} \tag{2}$$

III. Frictional Resistance

The geometric workspace is described in Section II-C. However, the frictional resistance at the arc prismatic pair influences the workspace, particularly in the pitch direction.

Therefore, in Section III, the movable range in the pitch direction is derived for the case in which frictional resistance exists at the arc prismatic pairs.

A. Rail Sliding Condition

When defining the friction coefficient at the arc prismatic pair as μ and the angle between the input direction and rail slide direction as β as shown in Fig. 4, the condition under which the rail starts to slide is described by (3). Furthermore, (3) is arranged into (4) considering the balance of force.

$$F_{in}\cos\beta \geq \mu N. \tag{3}$$

$$\frac{1}{\tan\beta} \geq \mu. \tag{4}$$

Both friction coefficient μ and angle β are important factors for the sliding of the arc prismatic pair.

B. Pressure Angle

In this study, the angle β is the called pressure angle. The pressure angle changed during pitching because the proposed mechanism was based on a differential drive.

By applying spherical trigonometry, the pressure angle is described as (5) corresponding to the input block positions φ_1 and φ_2.

$$\beta = \sin^{-1}\left(\frac{\cos\frac{\alpha}{2}}{\cos\frac{\varphi_1-\varphi_2}{2}}\right). \tag{5}$$

The pressure angle β depends on the rail intersection angle α and the pitch angle θ_{p} because it is certain from (1) that φ_1-φ_2 is a term that determines θ_{p}.

C. Pitch Movable Limit

The movable limit in the pitch direction can be calculated based on the rail-sliding condition. The end-effect pitch posture becomes the movable limit when the pressure angle β reaches maximum, that is, when (6) is satisfied.

$$\frac{1}{\tan\beta} = \mu. \tag{6}$$

Using (5) and (6), (1) can be transformed into an equation without φ_1-φ_2 and β, and the pitch movable limit $\theta_{\mathrm{p,max}}$ is described as (7).

$$\theta_{p,\max} = \sin^{-1}\left(\frac{\sqrt{\frac{1}{\mu^2+1} - \cos^2\frac{\alpha}{2}}}{\sin\frac{\alpha}{2}}\right). \tag{7}$$

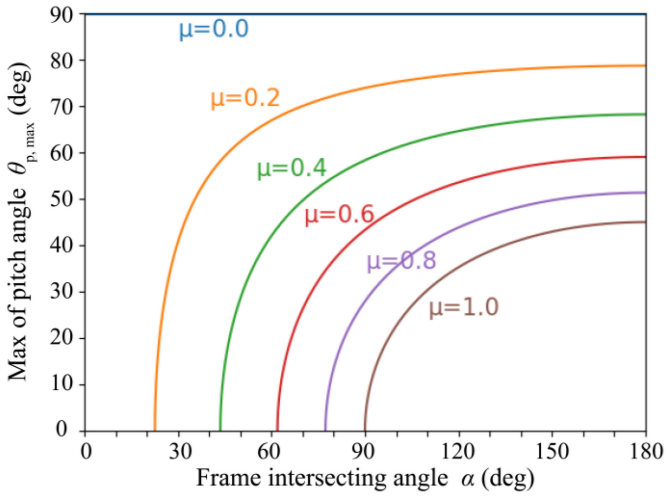

Fig. 5. Maximum pitch output rotation angle considering the frictional resistance.

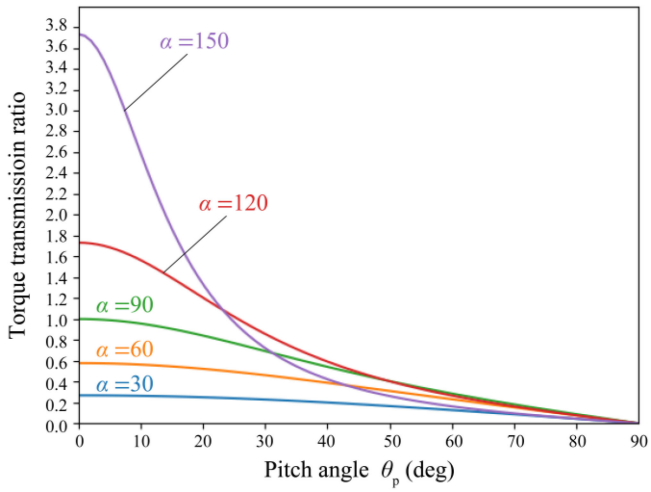

Fig. 6. Continuous variation of the torque transmission ratio depending on the end-effector orientation.

Thereafter, the limit depends on the rail intersection angle and friction coefficient. The limit was determined as shown in Fig. 5.

The smaller the friction coefficient is, the closer the pitch movable limit is to 90°. Therefore, it is desirable to reduce the friction at the arc prismatic pair by utilizing a rolling guide mechanism such as a roller slider.

In addition, the larger the rail intersection angle is, the larger the limit is. However, the effect gradually decreased and eventually converged to a certain value.

IV. Torque Transmission

For the proposed mechanism, the torque transmission characteristics differ between the roll and pitch operation, because the drive method differs between them. Considering only the roll operation, the input-output torque relation is always constant regardless of the posture, ignoring the weight of the parts. However, the relationship changes depending on posture when considering only the pitch operation.

In Section IV, the torque transmission ratio is formulated and it is confirmed that the ratio changes as the pitch angle increases. The torque transmission ratio is the ratio of the output torque to the total input torque; therefore, the ratio is a useful value for calculating the input torque required to obtain the target pitch angle output in advance.

The torque transmission ratio is described as (8) from the principle of virtual work because the work balance is held during pitch operation assuming static motion. (8) express the torque transmission ratio when the radius of the end effector is R.

$$\begin{aligned} ratio &= \frac{T_{E,pitch}}{|T_A| + |T_B|} = \frac{R \times F_{E,pitch}}{|R \times F_A| + |R \times F_B|} \\ &= \frac{F_{E,pitch}}{|F_A| + |F_B|} = \frac{d\left(\frac{\varphi_1 - \varphi_2}{2}\right)}{d\theta} \\ &= \cos\frac{\varphi_1 - \varphi_2}{2}\left(\frac{\cos^2\frac{\varphi_1 - \varphi_2}{2}}{\cos^2\frac{\alpha}{2}} - 1\right)^{\frac{1}{2}}. \end{aligned} \tag{8}$$

T_{A} and T_{B} refer to the input torque given to the entire mechanism from input blocks A or B, and $T_{\mathrm{E,pitch}}$ is the pitch output torque. F_{A} and F_{B} refer to the input force given to the input blocks A or B.

The ratio changes continuously as the pitch angle increases, as shown in Fig. 6, depending on the rail intersection angle.

In order to output the torque $T_{\mathrm{E,pitch}}$ in the pitch direction of the end effector, the total input torque $T_{\mathrm{In,total}}$ described as (9) is needed. d_{b}, d_{c} are the distances from the center of rotation to the center of gravity of the input blocks or the central block. W_{b} and W_{c} are the gravity applied to the input blocks or the central block.

$$\begin{aligned} &T_{In,total} \\ &= |T_A| + |T_B| + W_b d_b \left(\sin\varphi_1 + \sin\varphi_2\right) + W_c d_c \sin\theta_r \\ &= \frac{T_{E,pitch}}{ratio} + W_b d_b \left(\sin\varphi_1 + \sin\varphi_2\right) + W_c d_c \sin\theta_r. \end{aligned} \tag{9}$$

It should be noted that the net output torque is described by (10) if the center of gravity of the end-effector is d_{E} away from the center of rotation and the gravity of W_{E} is applied to the center of gravity.

$$T_{out} = T_{E,pitch} - W_E d_E \cos\theta_p. \tag{10}$$

V. Prototype Fabrication

In this study, we fabricated a prototype by replacing each part of the resin prototype [22] with a metal, as shown in Fig. 1. The prototype was designed to ensure that it was movable when an external force was applied to it for the experiment. The CAD model of the prototype is as shown in Fig. 7. The main parameters of the proposed prototype are listed in Table I.

The end-effector was fabricated by cutting highly rigid stainless steel SUS304. This fabrication suppresses deformation and ensures a highly accurate posture because the end-effector posture is controlled according to the geometric conditions of

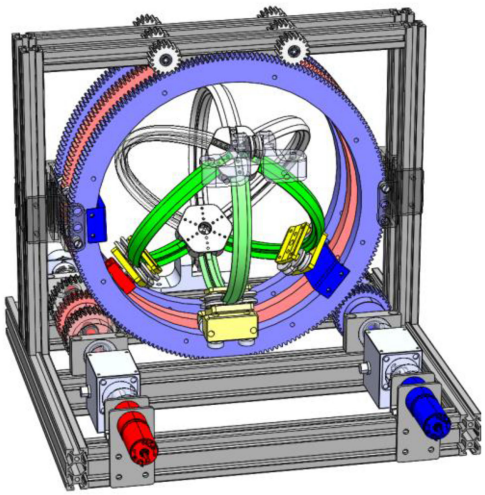

Fig. 7. CAD model of the prototype embodying 2-DOF SPM with arc prismatic pairs driven by a differential drive.

TABLE I
MAIN PARAMETERS OF THE PROPOSED PROTOTYPE

Whole	Height	355	mm
	Weight	385	mm
	Depth	370	mm
End effector	Weight	273	g
	Radius	102	mm
	Arc frame interval	60	deg

the end-effector shape and the position of the input blocks in proposed mechanism.

The ring gear is fabricated by cutting the spur gear of the S45C and hollowing out the center.

Two measures were taken to reduce the frictional resistance between the rail and roller slider. First, the arc prismatic pair is embodied by a roller slider, and second, the rail surface is electroless Ni-P-PTFE plated to achieve excellent lubricity and wear resistance.

The roller slider consists of four guide rollers arranged along the rail arc. The guide roller was made of aluminum A5052, and its surface was coated with an anodic oxide. The roller had a V-groove that corresponded to the cross-sectional shape of the rail.

To obtain a stable pitch output, the rail intersecting angle α is designed to be 120° degrees as a result of considering the change in the torque transmission ratio as shown in Fig. 6.

VI. DRIVING TORQUE MEASUREMENT

The actual driving torque was measured experimentally using a metal prototype, as described in Section VI. Thereafter, we clarified how the torque transmission ratio changes during pitch motion according to the end-effector posture.

To measure the torque transmission ratio, we measured the sum of the input torques during pitch motion while the end-effector was loaded with a constant torque in the pitch direction.

In addition, the influence of the rolling friction resistance on driving was evaluated by comparing the experimental and theoretical values. The influence cannot be theoretically estimated because the actual contact state between the roller and rail is unpredictable in the case where the roller slider is composed of V-groove guide rollers, as in the case of the prototype.

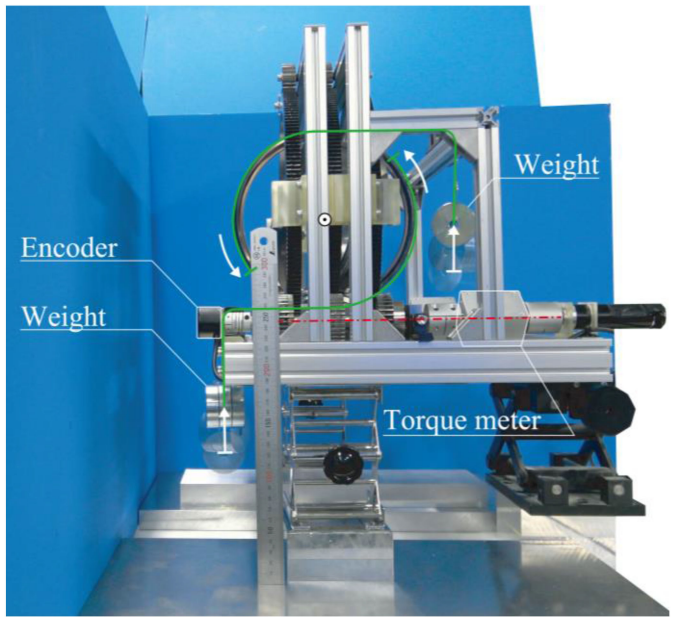

Fig. 8. Metal prototype with a weight and a torque meter.

A. Experiment Setup

A metal prototype was set up for the experiment, as shown in Fig. 8. The end-effector has six rails connected at the poles so that the end-effector becomes spherical. Therefore, the center of gravity and center of rotation match each other in the end-effector.

To load a couple of forces to the end-effector in the pitch direction by the gravity of the weights, two stainless wires are symmetrically wound around the center rail, and the two weights are attached to the end of the wires. These wires were hung on an aluminum pulley with a V-groove in the middle.

The weight was changed with to a width of 400 g at equal intervals, from 0 g (without weight) to 1200 g.

To control the motor speed, absolute encoders were attached to the rotary shaft of the spur gears via couplings. These encoders were made by the Microtech laboratory, the model number was MAS-20-1024G1, and the resolution was 1024/rotation.

To measure the input torques required for driving, that is, the torques around the motor drive shafts, torque meters were introduced and connected between the motor and the rotating shaft of the spur gear through couplings. These torque meters are made by UNIPULSE, and the model number is UTM-II-10Nm.

B. Experiment Method

The end-effector was rotated in the pitch direction according to the procedure below:

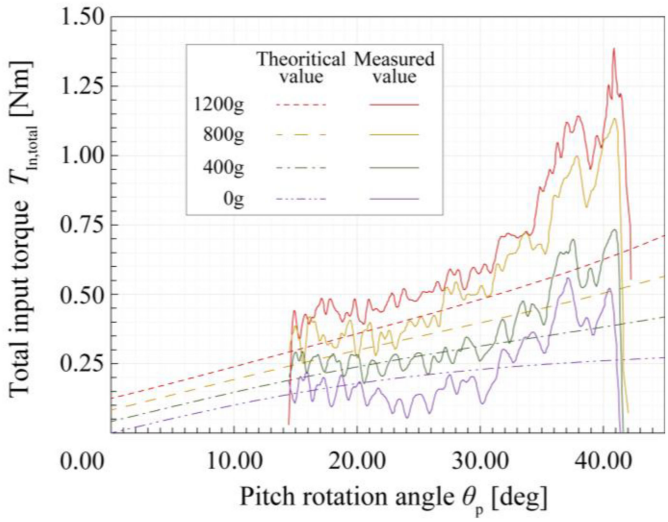

Fig. 9. Input torque required for pitch motion.

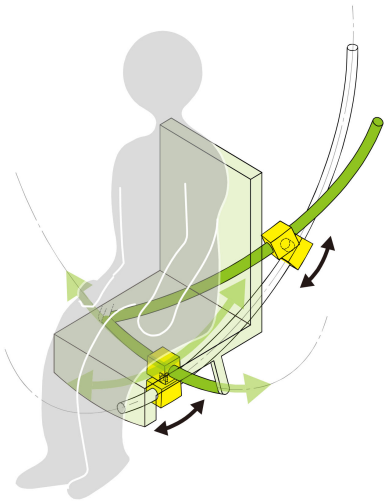

Fig. 10. Image of applying curved biaxial mechanism to a sheet.

e end-effector.

1) Input blocks A and B were rotated until the pitch angle was 42°. This is the initial state.
2) The input part blocks A and B were then rotated in different directions, and the end-effector was rotated in the pitch-negative direction.
3) The motion was then stopped when a pitch angle was 14.3°.

Simultaneously, the torque values around the motor drive shafts were recorded using torque meters. The measured torque values were converted to the driving torque for input blocks A and B, considering the gear ratio between the spur gear and ring gear.

In this way, it is clarified how driving torque is required to change the end-effector posture when a constant output torque in the pitch direction is obtained from this mechanism.

C. Experimental Results

Typical experimental results of the experiment are shown in Fig. 9. The horizontal axis is the estimated pitch angle θ_{p} which is calculated from the rotation numbers recorded by the encoders. The vertical axis is the total torque given to input blocks A and B, which is calculated from the torque values measured using torque meters.

The solid lines represent the experimental results. The dashed and dotted lines show the theoretical values calculated using (9).

When the weight was 400 g, 800 g, or 1200 g, the total driving torque reached a maximum immediately after the end- effector posture changed from the initial state. In the case of the 400 g weight, the maximum value was 0.73 Nm. In the case of 800 g, it was 1.13 Nm. In the case of 1200 g, it was 1.39 Nm.

Thereafter, the total driving torque gradually decreases as the pitch angle decreases. This phenomenon means that the torque transmission ratio (rate of output torque to input torque) changes according to the end-effector posture because the total input torque changes although the output torque is constant.

Additionally, the experimentally observed phenomenon represents the feature obtained from the principle of virtual work in (8).

The error between the measured and theoretical values is small in the range of small pitch angles and vice versa. It was experimentally confirmed that the influence of the rolling friction of the guide roller on driving became more pronounced as the pitch angle increased, and the energy loss increased.

VII. Conclusion

In this study, the influences of friction of the arc prismatic pair were confirmed by considering the slider-type differential -drive 2-DOF SPM. First, we theoretically confirmed the influence of the friction of the arc prismatic pair on the workspace of the SPM and the arc slider was designed to ensure the high smoothness. Second, the actual driving torque is experimentally measured and the influence of friction on driving is examined using the prototype embodying a slider-type differential-drive 2-DOF SPM.

We solved the rail sliding condition theoretically and consequently it was important to make the friction coefficient smaller to ensure high movable range in pitch direction in the case of the slider-type 2-DOF SPM. Based on this result, we design and fabricated arc slider using roller guides to reduce the friction at the arc prismatic pair.

The actual driving torque was measured experimentally using a metal prototype and we observed how the torque transmission ratio changes during pitch motion according to the end-effector posture. In addition, the influence of the rolling friction resistance was experimentally evaluated. The influence is difficult to be theoretically estimated in the case where the roller slider is composed of V-groove guide rollers, however the influence was evaluated by comparing the experimental and theoretical values of the input torque.

We plan to install the proposed mechanism in automobiles and apply it to the stabilization platform and the acceleration reduction mechanism [27], as shown in Fig. 10.

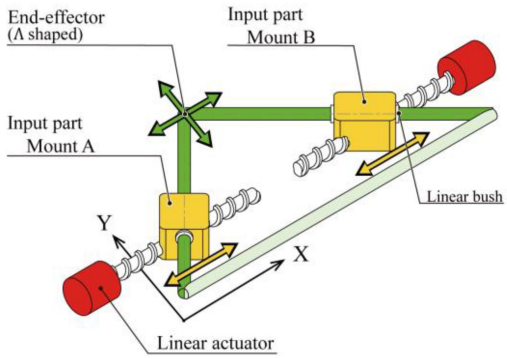

Fig. 11. Arrangement of links and couples constituting the slider-type 2-DOF planar parallel link mechanism.

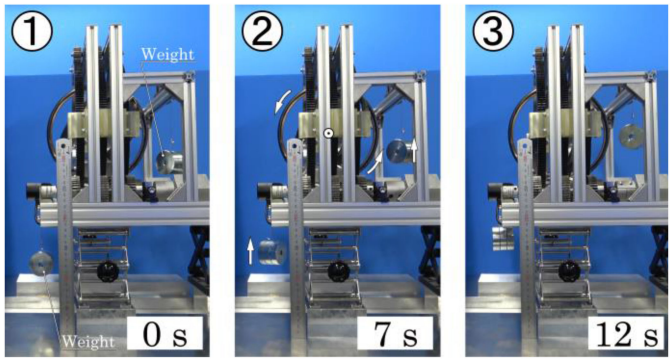

Fig. 12. Pitch operation procedure.

APPENDIX

The slider-type 2-DOF planar parallel link mechanism is used in a haptic 2-DOF buttock skin stretch device [25]. The arrangement of links and couples constituting the mechanism is as shown in Fig. 11.The experiment procedure in Section VI is as shown in Fig. 12.

REFERENCES

[1] C. M. Gosselin and F. Caron, "Two degree-of-freedom spherical orienting device," U.S. Patent 5 966 991, Oct. 19, 1999.

[2] G. R. Dunlop and T. P. Jones, "Position analysis of a two DOF parallel mechanism - The Canterbury tracker," *Mech. Mach. Theory*, vol. 34, no. 4, pp. 599–614, May 1999, doi: 10.1016/S0094-114X(98)00020-2.

[3] J. Zheng, J. Shi, Z. Zhang, X. Shi, and W. Li, "Workspace and kinematics analysis of a 2-DOF decoupled spherical parallel mechanism," in *Proc. 15th Int. Conf. Mechatron. Mach. Vis. Pract.*, 2008, pp. 403–407, doi: 10.1109/MMVIP.2008.4749567.

[4] M. E. Hesar, M. T. Masouleh, A. Kalhor, M. B. Menhaj, and N. Kashi, "Ball tracking with a 2-DOF spherical parallel robot based on visual servoing controllers," in *Proc. 2nd RSI/ISM Int. Conf. Robot. Mechatron.*, 2014, pp. 292–297, doi: 10.1109/ICRoM.2014.6990916.

[5] H. Su et al., "Cable-driven elastic parallel humanoid head with face tracking for autism spectrum disorder interventions," in *Proc. Annu. Int. Conf. IEEE Eng. Med. Biol.*, 2010, pp. 467–470, doi: 10.1109/IEMBS.2010.5626186.

[6] N. M. Bajaj, A. J. Spiers, and A. M. Dollar, "State of the art in artificial wrists: A review of prosthetic and robotic wrist design," *IEEE Trans. Robot.*, vol. 35, no. 1, pp. 261–277, Feb. 2019, doi: 10.1109/TRO.2018.2865890.

[7] K. Ueda, H. yamada, H. Ishida, and S. Hirose, "Design of large motion range and heavy duty 2-DOF spherical parallel wrist mechanism," *J. Robot. Mechatron.*, vol. 25, pp. 294–305, Apr. 2013.

[8] M. Ogata and S. Hirose, "Study on ankle mechanism for walking robots: Development of 2 d.o.f coupled drive ankle mechanism with wide motion range," in *Proc. IEEE/RSJ Int. Conf. Intell. Robot. Syst.*, 2004, vol. 4, pp. 3201–3206.

[9] R. Bsili, G. Metta, and A. Parmiggiani, "An evolutionary approach for the optimal design of the iCub mk.3 parallel wrist," in *Proc. IEEE-RAS 18th Int. Conf. Humanoid Robots*, 2018, pp. 475–482.

[10] W. A. Cao, S. J. Xu, K. Rao, and T. Ding, "Kinematic design of a novel two degree-of-freedom parallel mechanism for minimally invasive surgery," *J. Mech. Des. Trans. ASME*, vol. 141, no. 10, pp. 1–7, Oct. 2019.

[11] S. Ansari-Rad, M. Zarei, M. G. Tamizi, S. Mohammadi Nejati, M. T. Masouleh, and A. Kalhor, "Stabilization of a Two-DOF spherical parallel robot via a novel adaptive approach," in *Proc. 6th RSI Int. Conf. Robot. Mechatron.*, 2018, pp. 369–374.

[12] B. Danaei, M. Alipour, A. Arian, M. T. Masouleh, and A. Kalhor, "Control of a two degree-of-freedom parallel robot as a stabilization platform," in *Proc. 5th RSI Int. Conf. Robot. Mechatron.*, 2017, pp. 232–238.

[13] P. Feldman, T. Brumi, and G. Merri, "Motion platform system and method of rotating motion platform about plural axes," U.S. Patent 7 033 176 B2, Apr. 25, 2006.

[14] Y. Takeda, "Parallel mechanism," *Seimitsu Kogaku Kaishi/J. Jpn. Soc. for Precis. Eng.*, vol. 71, no. 11. pp. 1363–1368, 2005, doi: 10.2493/jjspe.71.1363.

[15] K. Maeda, S. Tadokoro, T. Takamori, M. Hiller, and R. Verhoeven, "On design of a redundant wire-driven parallel robot WARP manipulator," in *Proc. IEEE Int. Conf. Robot. Automat.*, 1999, vol. 2, pp. 895–900.

[16] A. Guerrouad and P. Vidal, "SMOS: Stereotaxical microtelemanipulator for ocular surgery," in *Proc. Images 21st Century. Annu. Int. Eng. Med. Biol. Soc.*, 1989, vol. 3, pp. 879–880.

[17] B. Danaei, A. Arian, M. Tale masouleh, and A. Kalhor, "Dynamic modeling and base inertial parameters determination of a 2-DOF spherical parallel mechanism," *Multibody Syst. Dyn.*, vol. 41, no. 4, pp. 367–390, 2017.

[18] L. J. Zhang, Y.-W. Niu, Y.-Q. Li, and Z. Huang, "Analysis of the workspace of spherical 2-DOF spherical 5R parallel manipulator," in *Proc. IEEE Int. Conf. Robot. Automat.*, 2006, pp. 1123–1128.

[19] T. Essomba and L. Nguyen Vu, "Kinematic analysis of a new five-bar spherical decoupled mechanism with two-degrees of freedom remote center of motion," *Mech. Mach. Theory*, vol. 119, pp. 184–197, Jan. 2018.

[20] X. Kong, "Forward displacement analysis of a 2-DOF RR-RRR-RRR spherical parallel manipulator," in *Proc. IEEE/ASME Int. Conf. Mechatron. Embedded Syst. Appl.*, 2010, pp. 446–451.

[21] J. J. Cervantes-Sánchez, J. C. Hernández-Rodríguez, and E. J. González-Galván, "On the 5R spherical, symmetric manipulator: Workspace and singularity characterization," *Mechanism Mach. Theory*, vol. 39, no. 4, pp. 409–429, 2004.

[22] N. Saiki et al., "2-DOF Spherical parallel mechanism capable of biaxial swing motion with active arc sliders," *IEEE Robot. Automat. Lett.*, vol. 6, no. 3, pp. 4680–4687, Jul. 2021.

[23] J. Enferadi and A. A. Tootoonchi, "A novel spherical parallel manipulator: Forward position problem, singularity analysis, and isotropy design," *Robotica*, vol. 27, no. 5, pp. 663–676, 2009.

[24] H. Kang and J. T. Wen, "Robotic assistants aid surgeons during minimally invasive procedures," *IEEE Eng. Med. Biol. Mag.*, vol. 20, no. 1, pp. 94–104, Jan./Feb. 2001.

[25] A. Horie, A. Nomura, K. Tadakuma, M. Konyo, H. Nagano, and S. Tadokoro, "Enhancing haptic experience in a seat with Two-DoF buttock skin stretch," in *Proc. Int. AsiaHaptics Conf.*, 2019, pp. 134–138.

[26] J. Craig, "Spatial transformations," (in Japanese) in *Robotics — Mechanism/Kinematics/Control—*, M. Nanjyo, 1st ed., Tokyo, Japan: Kyoritsu Shuppan, 1991, ch. 2, sec. 8, pp. 45–46.

[27] M. Nobutoki and S. Suzuki, "Development of a tilting system for reducing horizontal acceleration in cars," in *Proc. Soc. Automot. Engineers Jpn. Autumn Meeting*, 2019.